33rd Annual International Conference of the IEEE EMBS
Boston, Massachusetts USA, August 30 - September 3, 2011

Osteophyte Detection for Hand Osteoarthritis Identification in X-ray Images using CNNs

Sreeparna Banerjee, Satyajit Bhunia and Gerald Schaefer

Abstract— **In this paper we describe a class of analog algorithms based on the concept of cellular neural networks (CNNs) for detecting osteoarthritis (OA) from x-ray images. The indicator of OA that we examine is the presence of bony spurs or osteophytes in the vicinity of the weight bearing joints of the fingers. Results on a series of hand x-ray images are shown to be promising.**

I. Introduction

Osteoarthritis (OA), also known as Degenerative Joint Disorder (DJD), generally afflicts people over the age of 65 and is caused by the wear and tear of weight bearing joints such as hands, knees, hips and spine, causing a breakdown of the joint cartilage as well as texture variations of surrounding bone tissues. The main diagnostic imaging techniques to detect OA include x-ray imaging and MRI; x-ray imaging is preferred to MRI due to affordability and availability. In x-ray images, the effect of this OA shows up as intensity variations in the hard tissues, joint space narrowing, bony spurs as well as trabecular patterns on the surrounding bones [1].

Cellular Neural Network (CNN) [2], [3] based algorithms provide a useful approach when fast and robust preprocessing is required. Several applications in biomedical imaging using CNNs have been proposed in the literature [4], [5], [6]. The analogic cellular computer paradigm has revolutionised the processing of analogue array signals [2]. Its core comprises of a cellular nonlinear neural network, which is an array of analogue dynamic processors or cells. Partial differential equation based techniques are becoming the state of the art procedures in modern image processing [2].

In the case of analogic CNN computers, these are simple instructions like multiplication, addition, XOR, NAND, etc. In this paper, we apply these techniques to extract regions of interest in x-ray images of osteoarthritic hand joints. The remainder of the paper is organised as follows: Section II gives a brief overview of related work. Section III outlines the theory of CNNs, while Section IV relates our proposed algorithm. Section V gives experimental results and discussions, followed by conclusions in Section VI.

II. Related work

Signatures of OA that are seen in x-ray images include osteophytes, joint space narrowing, subchondral sclerosis, trabecular patterns in bone adjoining the cartilage and presence of cysts. In the following, emphasis will be laid on osteophytes, an example of which is given in Fig. 1.

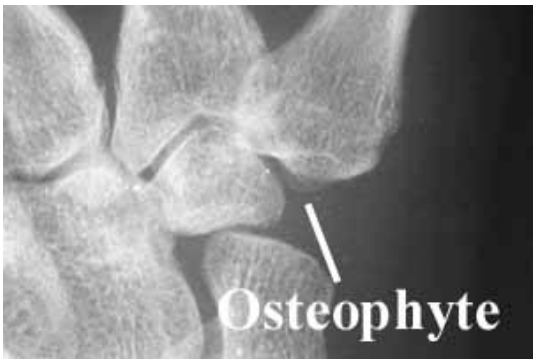

Fig. 1. Sample image of an osteophyte.

Although the major effort of research in OA detection in the hand from X-ray images has focussed on joint space narrowing (JSN), there have been several efforts to extract osteophytes and detect sclerosis. The distinct anatomical stages of hand OA have been described and characterised radiographically as progressing through sequential phases from normal to osteophyte formation, progressive loss of joint space and joint remodelling [7]. The hand can be evaluated with anterio-posterior and oblique views, although more detail can be obtained with magnified views of the specific joint. Such magnified views are useful in the evaluation of the soft tissues and fine detail of a specfic bone.

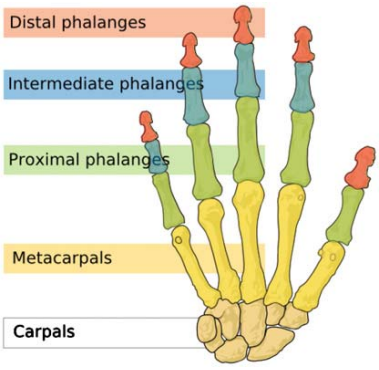

Fig. 2. Anatomy of the hand

Three regions of interest can be identified in the hand pathology concerning OA (see Fig. 2). The first one is the metacarpophalangeal joint (MCP joints between the

S. Banerjee is with the Natural Sciences Department, West Bengal University of Technology, Calcutta, India.
S. Bhunia is with the Department of Applied Electronics and Instrumentation, College of Engineering and Management, Kolaghat, India.
G. Schaefer is with the Department of Computer Science, Loughborough University, Loughborough, U.K.

metacarpal bones and proximal phalanxes). The proximal interphalangeal joints (PIP joints between the proximal and middle phalanxes) constitute the second region of interest, while the third set comprises distal interphalangeal joints (DIP joints between the middle and distal phalanxes). There are neither PIP nor DIP joints in the first finger due to the fact that there are only two phalanxes, proximal and distal and the only joint between the phalanxes is called the interphalangeal (IP) joint. The most commonly involved joints in the hand and wrist are the first carpometacarpal joints, the trapezionavicular joints and proximal interphalangeal and distal interphalangeal joints. Joint space loss is non-uniform and asymmetric. Assessing joint space width in a diagnostic process requires taking into account the distribution of narrowed hand joints (MCP, PIP and DIP) and their symmetry. Buckland-Wright *et al.* [8] demonstrated three symptoms, namely, subchondral sclerosis, joint space narrowing and osteophytes in 25 of 32 patients with hand OA during the 18 months of their study. Microfocal radiographic assessment of progression in hand OA [9] was studied and changes of four different features - subchondral sclerosis, number of osteophytes, juxtaarticular radiolucencies and JSN - over a period of 18 months recorded. It was concluded that bony changes progress significantly before occurrence of radiographically evident JSN. Pioneering efforts of van't Klooster *et al.* [10] and Bielecki *et al.* [11] have involved the detection of interphanlangeal and metacarpophalangeal joints and measuring the joint space widths (JSW) after obtaining contours of the fingers using appropriate image processing techniques. We have consolidated our earlier research on extracting osteophytes [12] using CNN algorithms from hand x-ray images and implemented an evaluation scheme for this detection algorithm.

III. Theory of CNNs

A standard CNN architecture consists of a rectangular $M \times N$ array of cells $C(i,j)$ with Cartesian co-ordinates (i,j) for $i = 1, 2, \cdots, M, j = 1, 2, \cdots, N$. For a digital image, this constitutes the rectangular/square array of pixels, with each cell corresponding to a pixel. Each cell $C(i,j)$ is defined by the state equation [2]

$$\begin{aligned} \dot{X}_{ij} &= -X_{ij} + \sum_{C(kl)\in S,(ij)} A(i,j;k,l)Y_{kl} \qquad (1) \\ &+ \sum_{C(kl)\in S,(ij)} B(i,j;k,l)U_{kl} + Z_{ij} \end{aligned}$$

where X_{ij}, U_{kl}, Y_{kl}, $Z_{ij} \in \Re$ are called state, input, output and threshold of cell $C(i,j)$ respectively, $A(i,j;k,l)$ and $B(i,j;k,l)$ are the feedback and input synaptic operators (or templates) and S_r is the sphere of radius r around cells. The radius r of a cell is a neighbourhood of cells. A 3×3 neighbourhood for which $r = 1$ is often chosen, though some applications require a 5×5 $(r = 2)$ neighbourhood.

A cellular neural network is space-invariant or isotropic if and only if both the synaptic operators $A(i,j;k,l)$ and $B(i,j;k,l)$ and threshold Z_{ij} do not vary with space. In the image processing applications considered here, both A and B as well as the threshold Z are considered to be both space and time invariant.

IV. Approach

Analogic CNN algorithms use CNN templates combined with logic operations for image processing. Templates used are essentially space invariant and time invariant synaptic operators A and B and a threshold Z in a 3×3 neighbourhood for which the sphere of influence has unit radius $(r = 1)$, although 5×5 $(r = 2)$ and 7×7 $(r = 3)$ neighbourhoods have also been used. Since mammograms are based on x-ray images, our procedures are somewhat similar to those in [4], [5] with some modification arising from the differences in the structures of interest (SOI) that we have isolated. Actual template values used depend on the particular screening and imaging system. We have tried several values but found that the values stated below gave the best results.

A. Osteophyte identification

Osteophytes or bony spurs are caused by the rubbing of bones with each other following the narrowing of joint space and wear and tear of the cartilage. In an x-ray image, these osteophytes would have thread-like structures with random orientations, located in the vicinity of joints and having dimensions of the order of a few millimeters. Thus, a modification of the spiculus seeker algorithm [5] has been used to isolate the osteophytes. The major differences are twofold: first, looping is not required to extract an annulus, and, second, since radial lines are not being extracted, the AVERAGE template is not used here.

The underlying steps are listed below:

1) Starting with black and white images both for input and initial states, an UNPEEL template is used to convert white pixels with black direct neighbours to black pixels. The template is given by:

$$A = \begin{bmatrix} 2 \end{bmatrix}$$

$$B = \begin{bmatrix} 0 & 0.3 & 0 \\ 0.3 & 0 & 0.3 \\ 0 & 0.3 & 0 \end{bmatrix}$$

$$Z = 2$$

   which has the effect of isolating threadlike structures near the joints.
2) A logical XOR operation is applied between the new and old kernels, followed by a segmentation algorithm using the REGION template which uses the synaptic operators $A = [1]$, $B = [-1]$ and $Z = 1$. Here, the input image is a black and white image displaying the thread like structures and the initial image is the original grey scale image.
3) With the help of the CHANGER template, black pixels are converted into zero valued grey ones. The synaptic operators for this operation are given by $A = [1]$, $B = [0.5]$, $Z = -0.5$.

4) Finally, we apply the LINE DETECTOR template to extract the almost linear, threadlike structures known as osteophytes. The templates are:

$$A = \begin{bmatrix} 0 \end{bmatrix}$$

$$B = \begin{bmatrix} -3 & -3 & -3 & -3 & -3 & -3 & -3 \\ -3 & -15 & -15 & -15 & -15 & -15 & -3 \\ -3 & -15 & 2 & 2 & 2 & -15 & -3 \\ -3 & -15 & 2 & 2 & 2 & -15 & -3 \\ -3 & -15 & 2 & 2 & 2 & -15 & -3 \\ -3 & -15 & -15 & -15 & -15 & -15 & -3 \\ -3 & -3 & -3 & -3 & -3 & -3 & -3 \end{bmatrix}$$

$$Z = \begin{bmatrix} 0 \end{bmatrix}$$

We tried the looping procedure with 1, 2, 15 and 30 loops, but found that one or two loops sufficed to isolate the bony structures.

Joints in hand x-ray images are located by first downscaling the image by a factor of 4 and the scanning the image with a window of size 15×15.

V. Results and Discussion

Experiments were carried out on nine images of the hand. Most parts of the images are background or irrelevant parts of bones with only a small area around the joint containing useful information pertaining to OA detection. Therefore, we choose small windows (20×20 pixels) while counting the ostephytes in the processed images. Fig. 3 shows an image of hands with OA and the extracted osteophytes, while Fig. 4 shows the results of different intermediate CNN operations on the image. Fig. 5 shows further images together with the extracted osteophytes.

Fig. 3. An image of hand with OA and extracted osteophytes

Fig. 4. Performing the CNN operation of blur, subtraction (BW and grey level) and XOR on the image.

The performance of our proposed method was evaluated by comparing the resulting osteophytes with radiologists' ground truth identification. Accordingly, we use the following two quantities:

$$\text{Sensitivity} = \frac{TP}{TP + FN} \tag{2}$$

$$\text{Accuracy} = \frac{TP + TN}{TP + FP + TN + FN} \tag{3}$$

$$\text{Specificity} = \frac{TN}{TN + FP} \tag{4}$$

where TP represents the number of osteophytes correctly detected, FN represents the number of osteophytes that were not detected, FP represents the number of osteophytes which were detected wrongly as osteophytes and TN represents the number of osteophytes which were correctly identified as non-osteophytes.

Fig. 5. Two further examples of hand with OA (left) and extracted osteophytes (right).

Of the nine images one did not have osteophytes. In the other images, the osteophytes were obtained. Table I gives the number of osteophytes identified and joints affected as well as a computation of sensitivity, specificity and accuracy of joints affected for the hand. The results indicate that osteophytes are accurately determined in 8 out of 9 cases,

Sl No.	Image size	TP	TN	FP	FN	Sensitivity(%)	Accuracy	Specificity	Joints affected
1	70 x 100	2	0	0	2	50	50	0	MCP
2	90 x 130	0	10	0	0	undefined	100	100	MCP
3	115 x 100	4	1	0	0	100	100	100	DIP, PIP.
4	140 x 225	1	0	0	0	100	100	undefined	carpal, MCP.
5	87 x 124	10	5	0	0	100	100	100	MCP
6	125 x 180	7	2	0	0	100	100	100	MCP, PIP.
7	140 x 221	3	0	0	0	100	100	undefined	
8	129 x 252	0	5	0	0	undefined	100	100	MCP
9	150 x 131	24	0	1	0	100	96	0	

TABLE I

TABLE OF OBTAINED RESULTS WITH JOINTS AFFECTED (DIP: DISTAL INTER-PHALANGEAL, PIP: PROXIMAL INTER-PHALANGEAL, MCP: METACARPO-PHALANGEAL)

whereas for the remaining one, deviations resulted from possible image artefacts. Sensitivity is excellent for 6 of the 9 cases and average for one case. Specificity is excellent for 5 of the 9 cases.

Osteophyte identification in the hip [13], thoracic region of the spine [14] and hand [8], using manual procedures to extract osteophytes, have been reported in the literature. In [8], osteophytes in the hand have been identified on quantitative microfocal radiographs, using cross wire cursors and osteophytes were detected in the juxtaarticular margins and pericapsular insertions of DIP, PIP and MCP joints. These manual identification procedures are often cumbersome and inaccurate. Our procedure, outlined above, is a semi-automated procedure for osteophyte detection in the hands, using CNN based algorithms. At present, the algorithm is suited for small subimages and we hope to improve for larger images. Also, osteophytes might not be detected if there are occlusions present.

VI. CONCLUSIONS AND FUTURE WORK

In this paper, we have presented a Cellular Neural Network based technique involing analogic (analog + logic) operations for osteoarthritis diagnosis. Results were shown to be accurate in over 90 percent of the images studied. We conclude that CNN based techniques hold much promise for extracting the signs of OA from x-ray images. This is more so since x-ray imaging is a suitable modality for capturing hard tissues like the bone and, therefore, irregularities in the bone structure can be well detected. Furthermore, we have shown that CNNs are capable of isolating small features of the order of a few millimeters such as osteophytes. These algorithms are suited for the diagnosis of this disease in hands where other indicators like joint space narrowing or textural changes in the surrounding bone are not so well manifested. In conclusion, CNN algorithms have been proved to be useful in OA detection, and it is hoped that with the present rapid advance in research and design of VLSI based array processors an accurate, fast and timely detection will become a reality. The procedure outlined in this paper for the detection of OA can be extended to other important weight bearing joints such as knees, hips and spinal column.

ACKNOWLEDGEMENTS

The first author would like to acknowledge support from AICTE, Government of India for a research grant (no.8023/BOR/RID/RPS- 110/7/8 of 5/3/08).

REFERENCES

[1] J.A. Lynch, D.J.Hawkes and J.C. Buckland-Wright, Analysis of texture in macroradio-graphs of osteoarthritic knees using the fractal signature, *Physics in Medicine and Biology*, Vol. 36,1991, pp. 709—722, and references therein.

[2] L.O. Chua and L. Yang, Cellular Neural Networks: Theory and Applications, *IEEE Transactions on Circuits and Systems*, Vol. 35, 1998, pp. 1257—1290.

[3] L.O. Chua and T. Roska, The CNN Paradigm, *IEEE Transactions on Circuits and Systems*, Vol.40, 1993, pp. 147—156.

[4] G. Liszka, T. Roska, A. Zarandy, J. Hegyesi, L. Kek and C. Rekeczky, Mammogram Analysis using CNN Algorithms, *SPIE-Medical Imaging* , Vol. 2434, 1995, pp.461—470.

[5] A.A. Zarandy and C. Rekeczky, Mammogram and Echo cardiogram Analysis via CNN Algo-algorithms, Proceedings ERCIM, 29, 1997, pp. 17—18.

[6] D. Matei and A. Matei, Detection of Diabetic Symptoms in Retina Images Using Analog Algorithms, *World Academy of Science, Engineering and Technology*, Vol. 45, 2008, pp. 408—411.

[7] G. Verbrugen and E.Veys, Numerical scoring systems for the anatomical evolution of Osteoarthritis of the finger joints, *Arthritis Rheum.*, Vol. 39, 1996, pp. 308-320.

[8] J.C. Buckland-Wright, D.G. Macfarlane and J.A. Lynch, Osteophytes in the osteoarthritic hand: their incidence, size, distribution and progression, *Ann. Rheum. Dis.*, Vol. 50, 1991, pp. 627-30.

[9] J.C. Buckland-Wirght, D.G. MacFarlane, J.A. Lynch and B. Clark, Quantitative microfocal radiographic assessment of progression in osteoarthritis of the hand, *Arthritis Rheum.*, Vol. 33, 1990, pp. 57-65.

[10] R. van't Klooster, E.A. Hendriks, I. Watt, M. Kloppenburg, J.H.C. Reiber and B.C. Stoel, Automatic quantification of osteoarthritis in hand radiographs: validation of a new method to measure joint space width, *Osteoarthritis and Cartilage*, Vol. 16, 2008, pp. 18—25.

[11] A. Bielecki, M. Korkosz and B. Zielinski, Hand radiographs preprocessing, image interpretation in the finger regions and joint space width measurements for image interpretation, *Pattern Recognition*, Vol. 41, 2008, pp. 3786—3798.

[12] S. Banerjee, G. Schaefer and I. K. Vlachos, Cellular Neural Network based algorithms in the early detection of hand osteoarthritis, *Proceedings FUZZ-IEEE*, 2009, pp. 1369—1373.

[13] A. K. Jeffery, Osteophytes and the Osteoarthritic Femoral Head, *J. Bone and Joint Surgery*, Vol. 57B, 1975, pp. 314-324.

[14] S. Otake, M. Takahashi and T. Ishikagi, Focal Pulmonary Interstitial Opacities Adjacent to Thoracic Spine Osteophytes, *American J Roentgenology*, Vol. 179, 2002, pp. 893-896.